HEAT-TRIGGERED SHAPE MEMORY EFFECT OF PEROXIDE CROSS-LINKED ETHYLENE–METHACRYLIC ACID COPOLYMER/NITRILE–BUTADIENE RUBBER THERMOPLASTIC VULCANIZATES WITH SEA-ISLAND STRUCTURE

YINGTAO SUN,[1] JIAHAO LI,[1] KERUI LIAO,[1] JING HUA,[2,*] ZHAOBO WANG[1,*]

[1]COLLEGE OF MATERIAL SCIENCE & ENGINEERING, QINGDAO UNIVERSITY OF SCIENCE & TECHNOLOGY, QINGDAO, 266042, P.R. CHINA

[2]KEY LABORATORY OF RUBBER-PLASTICS MINISTRY OF EDUCATION, QINGDAO UNIVERSITY OF SCIENCE & TECHNOLOGY, QINGDAO, 266042, P.R. CHINA

RUBBER CHEMISTRY AND TECHNOLOGY, Vol. 94, No. 3, pp. 449–461 (2021)

ABSTRACT

Designing shape memory polymers (SMPs) based on thermoplastic vulcanizates (TPVs) is an essential research topic. An efficient SMP is designed with typical sea-island structured ethylene–methacrylic acid copolymer/nitrile–butadiene rubber (EMA/NBR) TPVs in which the heat-control switched phase performed by the EMA phase is related to the shape fixity ability. The results show that the heat-triggered SMPs exhibit surprising shape memory properties (shape fixity >95%, shape recovery >95%, and fast recovery speed <30 s at the switching temperature of 95 °C). Through X-ray diffraction characterization, it is seen that the shape fixity of TPVs is achieved mainly through ethylene crystallization. The switching temperature is largely determined by the melting temperature (98 °C) obtained by differential scanning calorimetery. [doi:10.5254/rct.21.79926]

INTRODUCTION

Shape memory materials that have the ability to recover their permanent shape after fixing a temporary shape under external stimuli are considered to be "smart" materials. Several avenues, such as light,[1–4] pH,[5,6] electric field,[7–12] moisture,[13] and heat,[14–17] induce the shape memory effect in shape memory materials. Shape memory polymers (SMPs) have many advantages, such as low cost, portability, flexibility, good processability, controllable deformation and recovery temperature, and high elastic deformation,[9,18] as compared with other shape memory materials, such as shape memory alloys and ceramics. Because of their unique characteristics, SMPs can be broadly used in different fields, such as automobile engineering, aerospace engineering, deployable space structures, medical treatment, damage recovery, and other applications.[4,19–22]

SMPs as stimuli-responsive materials, that is, thermoresponsive shape memory polymers (HSMPs), are the most commonly investigated. The switching temperature in these SMPs can normally be the glass transition temperature (T_g) of the amorphous polymer or the melting temperature (T_m) of the crystalline polymer. The linear molecular structure of SMPs gives them the ability to diverse their permanent shape for different requirements.[23–25] SMPs rely on a polymer network cross-linked by covalent bond to reach a relatively high shape memory property other than materials with low plastic flow.[26–28] SMPs are deformed to a temporary shape, fixed by cool down, and then recover to their permanent shape at the T_g or T_m.[29–35] The typical cyclic program for HSMPs begins by heating the SMPs to a temperature near the T_g or T_m, namely, step 1. At this temperature, the polymer network can be easily motivated, and thus the SMPs can be changed into a temporary shape by applying an external stress. Then, in the presence of an applied load, the temperature is rapidly cooled below the T_g or T_m, at which the polymer chains are frozen to fix the

*Corresponding author. Email: Zhaobo Wang wangzhb.cn@gmail.com

Downloaded from https://prime-pdf-watermark.prime-prod.pubfactory.com/ at 2025-07-31 via free access

temporary shape, and the entropic elasticity is stored in the cross-linked network structure at this stage, as step 2.[15] In step 3, the HSMPs can recover to their original shape by repeating step 1.

Polymer blending is an alternative strategy for the development of new SMPs with optimized chemical and physical properties; this method is especially simple to achieve in comparison with the chemical synthesis method. Thermoplastic vulcanizates (TPVs) as a blend of a thermoplastic and a rubber form a cross-linked structure through dynamic vulcanization.[35–40] Dynamic vulcanization refers to the method of the selective vulcanization of the rubber phase in the melting-mixing process of thermoplastic polymer, which results in a two-phase material in which the cross-linked rubber phase is typically dispersed in a thermoplastic matrix in the form of particles. On one hand, the plasticity of the plastic phase makes the TPV shape fixable and changeable; on the other hand, the cross-linking of the rubber phase provides the resilience to improve the shape memory effect. TPVs, which consist of the thermoplastic phase and cross-linked rubber phase and exhibit excellent properties of the shape memory effect, are ideal shape memory materials. Generally, there have been many reports on HSMPs prepared by dynamic vulcanization. For example, the work by Yuan et al.[41] was the first to report on the SMP based on polylactic acid/natural rubber (PLA/NR) TPVs via dynamic vulcanization. Xu et al.[42] fabricated HSMPs based on PLA/ENR TPVs via peroxide-induced dynamic vulcanization. Xu et al.[43] constructed HSMPs based on polypropylene/ethylene-propylene-diene terpolymer (PP/EPDM) TPVs via zinc dimethacrylate (ZDMA) in situ compatibilization.

We recently reported dynamically vulcanized ethylene-vinyl acetate/nitrile-butadiene rubber (EVA/NBR) blends, in which the cross-linked NBR phase was uniformly distributed in the continuous EVA phase to form a typical sea-island structure.[35] In this research, by using a peroxide cross-linking agent, dicumyl peroxide (DCP), and a dynamic vulcanizing technology, ethylene–methacrylic acid (EMA)/NBR TPVs were first prepared for the research of heat-triggered shape memory. This article focuses on the remarkable shape memory behavior of EMA/NBR TPVs. With such a novel system, the nitrile groups in NBR render it more compatible with EMA, potentially providing stronger interfacial adhesion to support shape memory performance. The microstructure, thermomechanical properties, and shape memory behavior of EMA/NBR TPVs were investigated systematically and re expected to be applied in the field of sensors and automation devices.

EXPERIMENTAL

MATERIALS

EMA, injection grade AC1609 (a melt flow index [MFI] of 5.0 g/10 min, 9.0 wt.% methacrylic acid content), was supplied by DuPont Co., Ltd. (Wilmington, DE, USA). NBR, type 3305 (33 wt.% acrylonitrile content and ML_{1+4} [100 °C] = 45), was commercially manufactured by Lanzhou Petrochemical Co., Ltd. (Lanzhou, China). DCP, which was used as a vulcanizing agent, was obtained from Gaoqiao Petrochemical Co., Ltd. (Shanghai, China). Triallyl isocyanurate (TAIC) was used as an activator and obtained from Rhein Chemie Co., Ltd. (Cologne, Germany). N-Phenyl-2-naphthylamine (antioxidant D) was used as an antioxidant and obtained from Shengao Chemical Co., Ltd. (Caoxian, China).

PREPARATION OF EMA/NBR BLENDS

EMA, NBR, and the industry raw materials listed above were used to prepare the blends. The concentration of the cross-linked NBR system was expressed in percentage of rubber by weight (phr). The following ingredient was included in the recipe of the peroxide-containing accelerating system: 100 phr NBR, 2 phr DCP, 3 phr TAIC, 1 phr antioxidant D.

Downloaded from https://prime-pdf-watermark.prime-prod.pubfactory.com/ at 2025-07-31 via free access

TABLE I
COMPOSITION OF VARIOUS EMA/NBR TPVS

TPV No.	EMA, wt.%	NBR, wt.%	Designation
1	20	80	E2N8
2	30	70	E3N7
3	40	60	E4N6
4	50	50	E5N5
5	60	40	E6N4

A two-step mixing process was adopted to prepare the EMA/NBR TPVs. In the first step, to mix all ingredients evenly, the NBR and the ingredients were put into the interval between two rolls of a mill (X(S) K-160, Shanghai Qun Yi Rubber Machinery Co., Ltd., Shanghai, China) at room temperature. The preblend was removed from the mixer, and all ingredients were compounded evenly. In the second step, the compounds were prepared by melt mixing the NBR preblends with EMA resins using a mixer (SY-6215-AL, Shi Yan Precision Instruments Co. Ltd., Dongguan, China). The temperature of the mixer was maintained at 165 °C with a constant rotor (cam type) speed of 43 rpm. In detail, the whole process took 10 min, the NBR preblend was added to the melted EMA and mixed for 3 min, followed by another 7 min to allow for dynamic vulcanization, and finally the compounds were removed from the mixer. The compounds were preheated at 165 °C for 10 min in a plate vulcanizing machine (50 T, Shanghai Qun Yi Rubber Machinery Co., Ltd.) and then compression molded under a pressure of 15 MPa at 165 °C for 6 min, followed by cold compression in another molding machine (SK 2401, Kai Yuan Machinery Co. Ltd., Nanjing, China) for 8 min. Dumbbell-shaped test specimens were die-cut neatly from the compression-molded sheet. Details of the compositions of EMA/NBR TPVs are listed in Table I.

CHARACTERIZATIONS

Microscopy Analysis. — Field-emission scanning electron microscopy (FE-SEM; JSM-6700F, Japan Electron Optics Laboratory Co., Ltd., Tokyo, Japan), was used to study the morphology of etched samples in which the EMA phase was extracted by immersing TPV in toluene at 120 °C for 2.5 h, and the etched samples were then dried sufficiently at 40 °C. Before morphological observation, thin platinum layers were sputter-coated on the surface of the samples to prevent the accumulation of static charge.

Tensile Tests. — The tensile properties of dumbbell-shaped EMA/NBR TPVs specimens were characterized by a universal material testing machine (TCS-2000, GoTech Testing Machines Inc., Taiwan) under a crosshead speed of 500 mm/min according to ASTM D412.

Dynamic Mechanical Analysis. — Dynamic mechanical thermal analysis of specimens was carried out using an Eplexor 500N DMTS (NETZSCH GABO Instruments GmbH, Ahlden, Germany) under tensile mode. The specimens were tested over a temperature range of –40 to 110 °C at a heating rate of 3 °C/min in 10% strain mode. The test was performed at an oscillating frequency of 10 Hz to quantify the storage modulus (E') and loss tangent ($\tan\delta$).

Differential Scanning Calorimeter. — Using differential scanning calorimetry (DSC; TA-DSC-Q20, American TA Instruments Co., Ltd., Newcastle, DE, USA), the samples were analyzed in a nitrogen atmosphere. A sample of about 5–10 mg was heated to 120 °C at a rate of 20 °C/min and held at this temperature for 5 min to eliminate the effect of thermal history. The testing was conducted in the temperature range of –40 °C to 120 °C, and the temperature programmed rate was 20 °C/min.

Downloaded from https://prime-pdf-watermark.prime-prod.pubfactory.com/ at 2025-07-31 via free access

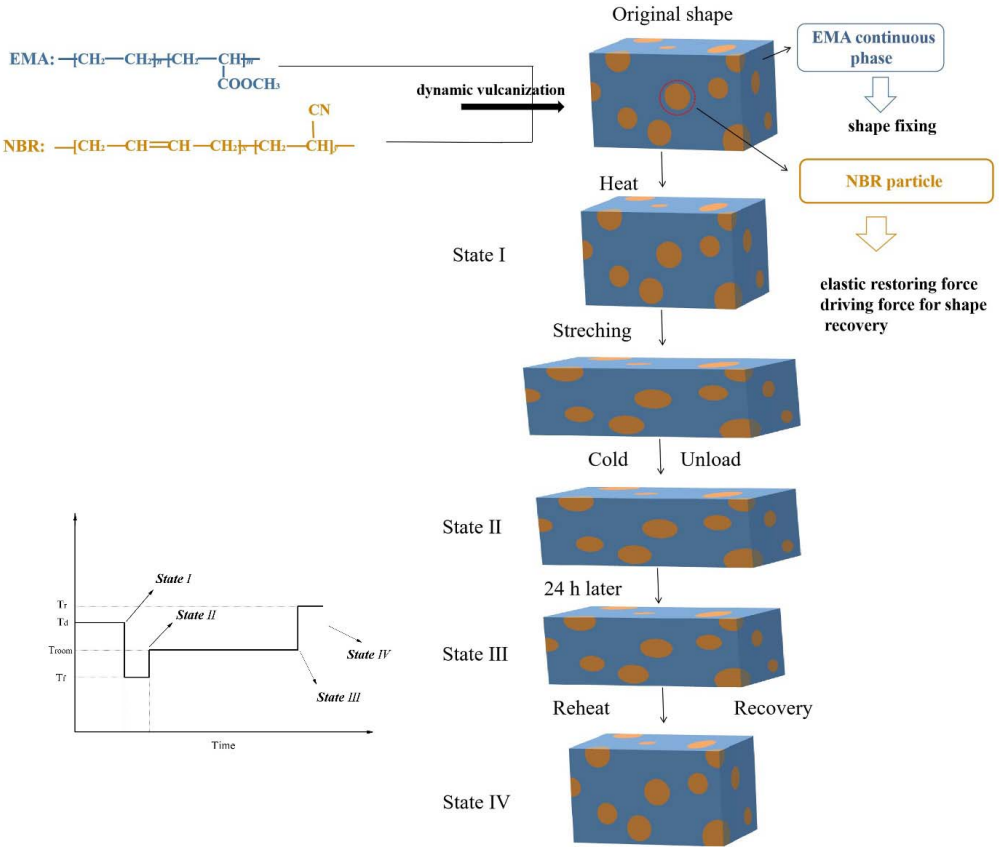

FIG. 1. — Schematic describing and illustration of SME measurement of EMA/NBR TPVs.

X-Ray Diffraction. — The crystal structures of the samples were further characterized and analyzed using X-ray diffraction (XRD; with Cu Ka radiation, $\lambda = 1.54178$ °, D/max-2500/PC, Rigaku Co., Ltd., Tokyo, Japan) at room temperature. The diffraction patterns were recorded in a scanning range from 5° to 50° (2θ) using a step scan mode with steps of 0.02° (2θ) and a time per step of 10 s.

SME Measurement. — The method of shape memory effect (SME) measurement tests was described by the report by Zhu and colleagues[44]: (1) an interval was marked that is 20 mm (L_0) at the center of the dumbbell specimen; (2) the marked dumbbell specimen was preheated under deformation temperature (T_d) for 10 min (State I); (3) an external force was placed to elongate the dumbbell specimen to the required length; (4) the deformed specimen was cooled to 1 °C under loading for 5 min, and the marked interval was recorded as L_1 (State II); (5) upon removal of the external force, the specimen was placed at room temperature for 24 h, and the marked interval was recorded as L_2 (State III); and (6) the specimen was heated at the recovery temperature (T_r) for 5 min, and the marked interval was recorded as L_3 (State IV). The schematic describing the SME measurement is shown in Figure 1. The shape fixity (SF) and shape recovery (SR) were calculated by using Eqs. 1 and 2, respectively. Each sample was measured for five individual specimens to reach an average value.

$$SF = \frac{L_2 - L_0}{L_1 - L_0} \times 100\% \quad (1)$$

Downloaded from https://prime-pdf-watermark.prime-prod.pubfactory.com/ at 2025-07-31 via free access

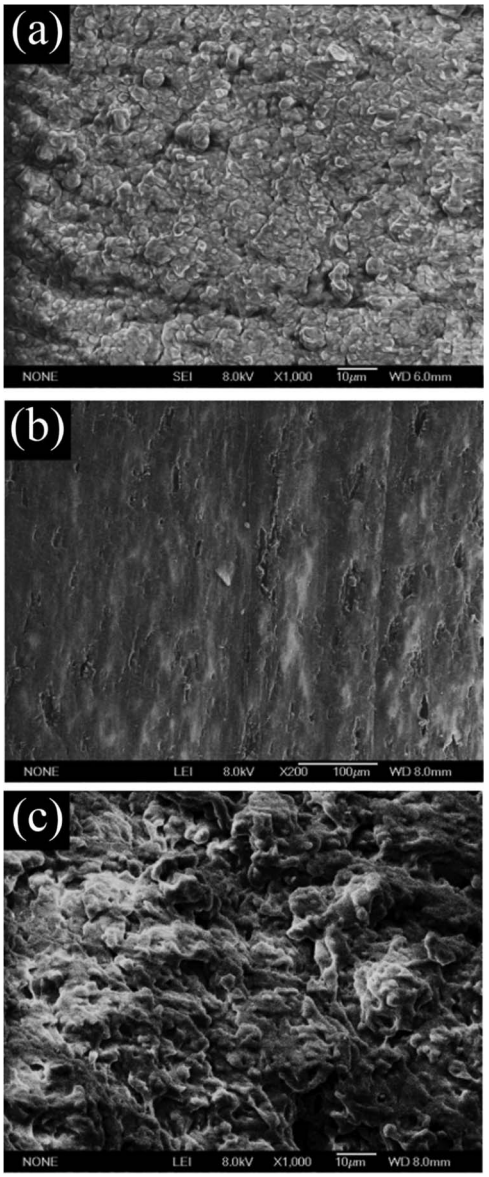

FIG. 2. — FE-SEM images of E5N5 specimen: (a) etched surface; (b) longitudinal stretching surface; (c) cryogenically fractured surface.

$$\mathrm{SR} = \frac{L_1 - L_3}{L_1 - L_0} \times 100\% \tag{2}$$

RESULTS AND DISCUSSION

MORPHOLOGY AND MICROSTRUCTURE OF EMA/NBR TPVs

To provide good insight into the phase morphology of TPVs, the surfaces of EMA/NBR (50/50) TPVs were etched, and their FE-SEM micrographs are shown in Figure 2. The EMA phase on

Downloaded from https://prime-pdf-watermark.prime-prod.pubfactory.com/ at 2025-07-31 via free access

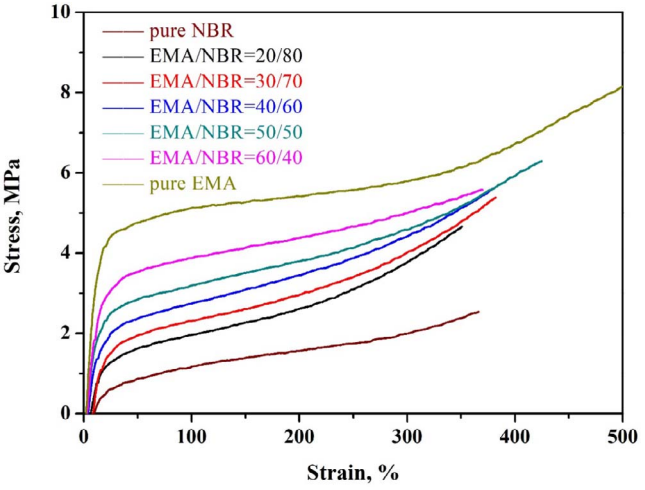

FIG. 3. — Stress–strain behaviors of EMA resin, NBR vulcanizate, and EMA/NBR TPVs.

the surface of the TPVs was resolved, whereas the cross-linked NBR domains remained and adhered to the surface. During dynamic vulcanization, the initiation of the cross-linking reaction increased the viscosity of the NBR phase quickly, and the shear force broke the NBR phase into dispersed particles.

Figure 2a shows that the cross-linked NBR particles dispersed evenly in the continuous EMA matrix phase and the dimensions of irregular-shaped NBR particles of EMA/NBR TPVs were about 3 μm to 5 μm. The FE-SEM image of the longitudinal stretching surface of E5N5 specimen is presented in Figure 2b. It should be noted that the tensile speed was set at 500 mm/min. A pronounced orientation texture appeared on the longitudinal stretching surface of the E5N5 specimen (Figure 2b), which was attributed to the successful fixation of the elongated NBR particles by the orientation of the crystalline region in the EMA phase. Figure 2c shows the cryogenically fractured surfaces of E5N5 specimen. The E5N5 specimen had a rough surface structure with some wrinkles, implying that good interfacial adhesion existed between the EMA and NBR phase.

In summary, Figure 2 indicates greater compatibility and higher interfacial adhesion between the EMA and NBR, which plays a crucial role in the shape memory behavior for the EMA/NBR TPVs.

MECHANICAL PROPERTIES

The test of shape memory effect needs to be carried out at a high temperature. TPV is thus required to have certain mechanical properties. The stress–strain curves of the NBR vulcanizate, dynamically vulcanized EMA/NBR blends, and pure EMA are presented in Figure 3, which shows that the pure EMA behaved like a tough plastic under the typical deformation processes. The modulus of the EMA/NBR blends increased with increasing EMA incorporation, indicating the hard and tough character of the EMA resin. The curved shapes of the EMA/NBR blends were basically similar and exhibited characteristics of a representative elastomer with soft and tough characters, whereas the NBR static vulcanizate had a much lower modulus and tensile strength.

Downloaded from https://prime-pdf-watermark.prime-prod.pubfactory.com/ at 2025-07-31 via free access

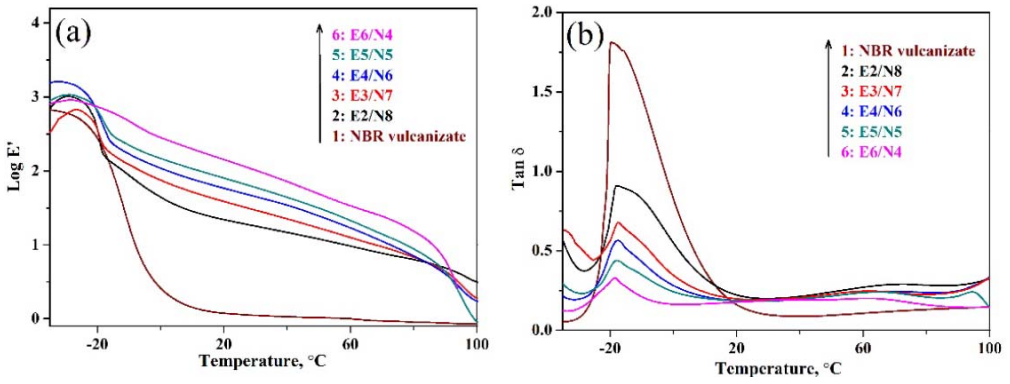

FIG. 4. — Dynamic mechanical analysis results of the storage modulus (E′) and loss tangent (tanδ) as a function of temperature of the NBR vulcanizate and EMA/NBR TPVs: (a) log E′; (b) tan δ.

To study the main thermomechanical relaxation of NBR vulcanizate and EMA/NBR TPVs, we performed DMTS analysis, and the storage modulus (E′) and loss tangent (tanδ) as a function of temperature of the specimens are presented in Figure 4a,b.

The temperature dependence of the E′ curves of the NBR vulcanizate and EMA/NBR TPVs are shown in Figure 4a. It can be observed that the E′ values of TPVs in the range of –40 to 110 °C could be obviously improved by increasing the dosage of EMA, which could be explained by the higher modulus of EMA. Compared with EMA/NBR TPVs, the E′ values of NBR vulcanizate exhibited a sharp transition step in the range of –20 to 0 °C with increasing temperature, which corresponded to the glass transition area of the NBR vulcanizate and meant that the cross-linked NBR phase was a soft elastomer at room temperature. In Figure 4b, the variation of tanδ with respect to temperature can be clearly observed, and the maximum peak values of the NBR vulcanizate and EMA/NBR TPVs were about –20 °C, which corresponds to the T_g of each component. Furthermore, there was only a single T_g value of each specimen and only a marginal change in the T_g of series EMA/NBR TPVs, which indicated that the two components constituted a well-compatible mixture in the TPVs.[45]

CRYSTALLINE STRUCTURES OF EMA/NBR TPVs

The crystalline melting temperature (T_m) and enthalpy of crystallization (ΔH) of series EMA/NBR TPVs were collected from the cooling curves and reheating curves in DSC, respectively, and are listed in Table II. Figure 5 shows that the increasing proportion of EMA in the various TPVs systems was reflected in their corresponding ΔH values, as there was a gradual and steady increase

TABLE II
T_m AND ΔH OF EMA/NBR TPVs

TPV No.	EMA, wt.%	NBR, wt.%	T_m, °C	ΔH, J/g
1	20	80	97.59	4.23
2	30	70	98.46	6.88
3	40	60	98.39	8.74
4	50	50	98.38	11.55
5	60	40	98.52	14.95

Downloaded from https://prime-pdf-watermark.prime-prod.pubfactory.com/ at 2025-07-31 via free access

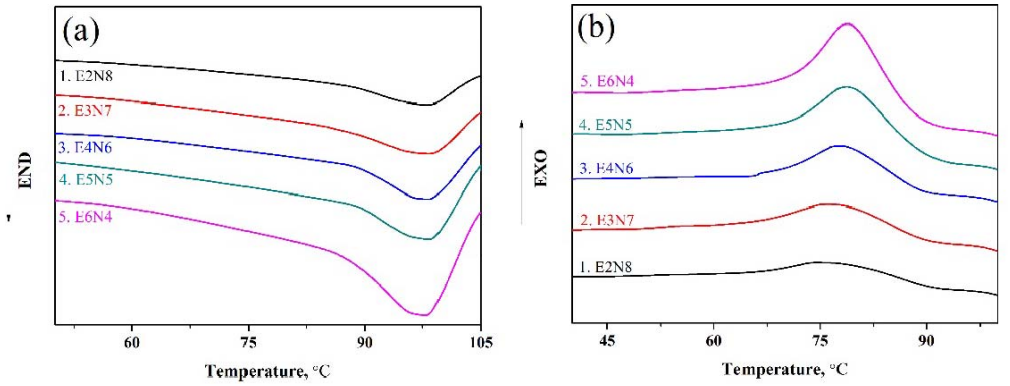

FIG. 5. — DSC heating (a) and cooling (b) curves showing the melting and crystallization of the EMA/NBR TPVs.

in ΔH with increasing EMA dosages and the value of ΔH jumps from the initial 4.23 J/g to 14.95 J/g at 60 phr EMA. In the present study, the increasing proportion of EMA in TPVs appeared to have a little effect on the crystallization temperature. The series TPVs in which the EMA as the matrix or continuous phase to hold the microdomains of NBR almost possess the identical crystallization temperature (T_c) and crystalline melting temperature (T_m). T_c and T_m were the thermal characteristics, which were controlled by the EMA matrix only. For the series of the TPVs, the EMA phase displayed a discrete peak in its T_m.[46]

The XRD patterns of pure EMA, series EMA/NBR TPVs are shown in Figure 6. For the pure EMA consisting of methacrylic acid and ethylene, three perceptible diffractive peaks were observed around 21.28°, 23.62°, and 36.08°, which corresponded to the typical (110), (200), and (020) crystallographic planes of polyethylene, indicating that EMA had an orthorhombic unit cell structure. Compared with the XRD curves of TPVs with low NBR content, the intensity of the diffractive peak would reduce with enhanced NBR content, indicating the decreasing crystalline

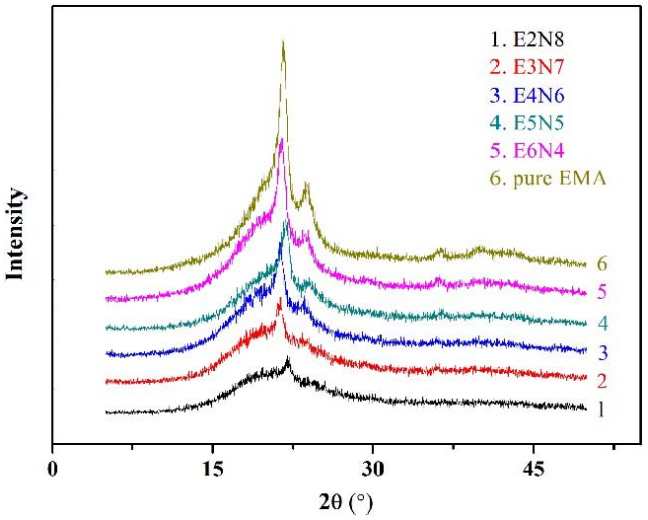

FIG. 6. — XRD patterns of pure EMA and EMA/NBR TPVs.

Downloaded from https://prime-pdf-watermark.prime-prod.pubfactory.com/ at 2025-07-31 via free access

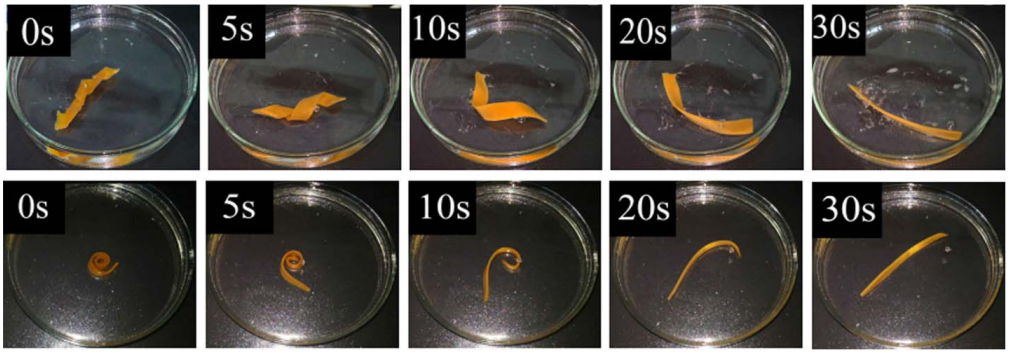

FIG. 7. — Shape memory behavior in various modes for E5N5, while both T_d and T_r were set at 95 °C.

structure content in EMA. This was generally in agreement with the reduction in mechanical properties in the TPVs with high NBR content.

SHAPE MEMORY BEHAVIOR OF EMA/NBR TPVS AND SHAPE MEMORY MECHANISM ANALYSIS

When changing the shape of the E5N5 specimens into a spiral and curled model, as shown in Figure 7, the SME properties of EMA/NBR TPVs can be directly seen. The SR was achieved at 95 °C after cooling down the deformation temperature of TPVs, which was also 95 °C, slightly lower than the T_m (98 °C) of the EMA resin, because the partial melting of the EMA crystal region softened the EMA/NBR TPVs, which deform easily at this temperature, and crystallized to fix the temporary shape of TPVs with little contraction. This was easily recovered from the varied temporary shape to the original shape of TPVs over time (∼30 s), demonstrating that the TPVs with E5N5 had fabulous reprocessing and shape reconstruction abilities during the process of shape memory.

The shape memory effect of EMA/NBR TPVs is deeply related to T_d, as shown in Figure 8. Through the various T_d values, the SF and SR of the series EMA/NBR TPVs were obtained under the same recovery temperature of 95 °C. Figure 8a shows that the SF increased with increasing EMA content in the EMA/NBR TPVs, indicating that the SF ability of the EMA/NBR TPVs was mainly determined by the EMA matrix phase. The strain–crystallization phenomenon under constant load was achieved by the anomalous cooling-induced elongation in the semi-crystalline

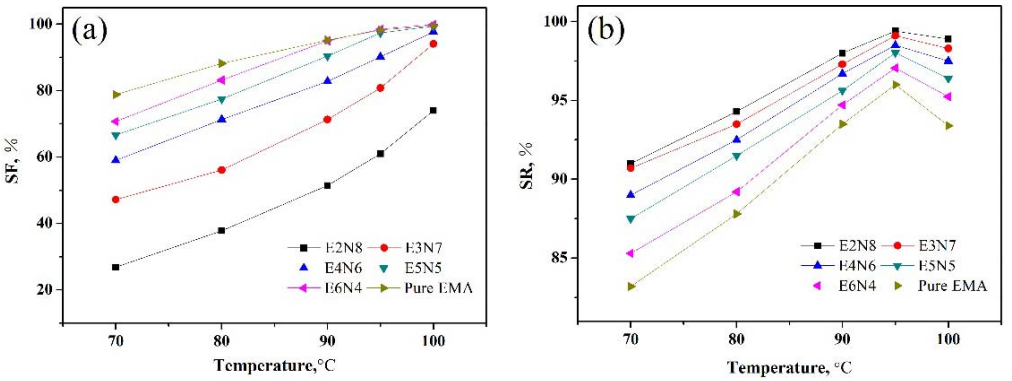

FIG. 8. — SF (a) and SR (b) ratios for the series of EMA/NBR TPVs obtained at various T_d values (T_r = 95 °C).

Downloaded from https://prime-pdf-watermark.prime-prod.pubfactory.com/ at 2025-07-31 via free access

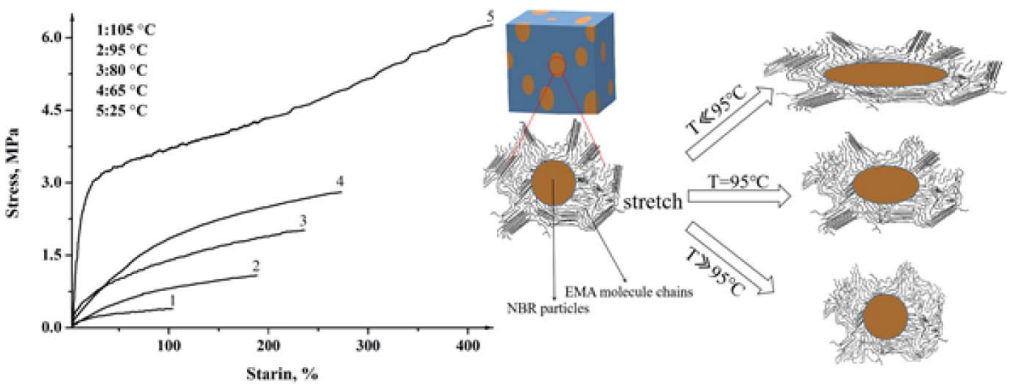

FIG. 9. — Stress–strain curves of E5N5 specimens at 25, 60, 80, 95, and 105 °C and a brief description of the deformation state of the NBR particles in the EMA phase.

EMA phase,[47] which was the primary cause why the elongated NBR particles could be fixed firmly. Figure 8a also shows that the SF increased with higher T_d, at which the rearrangement of the EMA phase can easily and quickly form a temporary shape. It should be noted that the SR in Figure 8b would be increased by increasing the T_d to lower than 95 °C, but would decrease sharply once the T_d passes 95 °C, caused by the decrease in NBR recovery ability after a large degree of deformation, which is discussed in Figure 9.

To investigate the effect of temperature on TPVs, the stress–strain curves of E5N5 specimens at 25, 65, 80, 95, and 105 °C were studied to help us understand the functions of phase structure in the shape memory mechanism. A brief description of the deformation state of the NBR particles in the TPVs is also presented, as shown in Figure 9. From Figure 9, we can see that the stress–strain curve of E5N5 at 25 °C demonstrates that the TPVs were soft and tough as typical elastomers. Both the tensile strength and the elongation at break would be decreased by rising the heat treatment temperature (no more than T_m), which is attributed to the fact that the temperature would, to some extent, enhance the activity of the chains and the order of the macromolecular chains in the EMA amorphous phase; in addition, to a large extent, the EMA molecule chains could hardly be set in motion. When the heat treatment was set at 95 °C (which is close to but still lower than the T_m of EMA), the TPVs showed a softening characteristic, due to the melting of the crystal region of the partial EMA. The TPVs could be deformed easily by applying external force; the orientation of the macromolecular chain would be frozen by cooling down the deformation temperature, which was why the TPVs had a higher SF. During the SR process, the potential energy of the NBR particles formed by the deformation was released, caused by the disorientation and melting of the EMA crystal region of TPVs to recovery of their original shape. When the test temperature was increased to 105 °C (above the T_m of EMA), the great increase in the melting crystal region of EMA would largely decrease the strength and massively reduce the elongation to 103%. This indicates that the TPVs can be used only at temperatures less than 95 °C. The EMA phase would be softened above this temperature, and the interface of EMA–NBR was too weak to fix the NBR particles forcefully, failing to provide enough recovery driving force and resulting in low SR, as shown in Figure 9.

To evaluate how the different values of T_r influence the SR for series EMA/NBR TPVs with a fixed T_d (95 °C), Figure 10 shows that the increase in NBR content would increase the SR of the EMA/NBR TPVs, due to the main recovery force provided by the NBR phase in TPVs. Specifically, the recovery force could be transported from the NBR particles to the EMA phase though the interface, because of the good compatibility between them. During the SF process, the NBR particles store large potential energy after the deformation of TPVs under external force.

Downloaded from https://prime-pdf-watermark.prime-prod.pubfactory.com/ at 2025-07-31 via free access

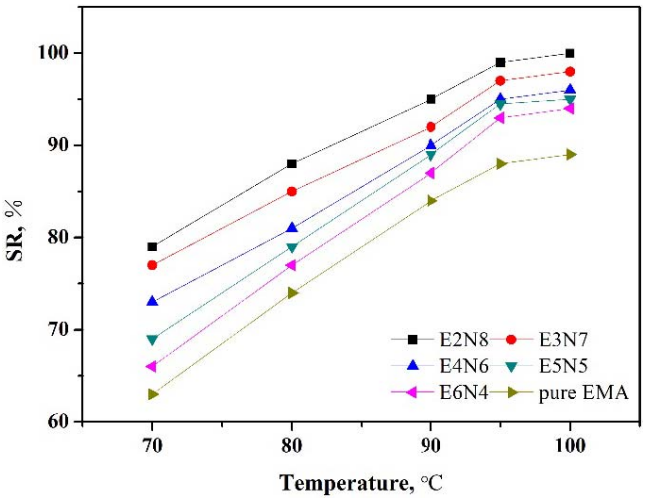

FIG. 10. — SR ratios for the series of EMA/NBR TPVs obtained at various T_r values ($T_d = 95$ °C).

During the SR process, the potential energy in the NBR particles can be released through the EMA–NBR interface to the EMA matrix, realizing the SR of TPVs.

To measure the effect of different stains on the shape memory performance of EMA/NBR TPVs, we performed shape memory testing on E5N5 specimens while both the temperature of fixation and recovery were set at 95 °C. The results are shown in Figure 11. According to Figure 11, a higher strain would lead to lower SF and recovery, caused by the larger deformation of NBR particles that requires better fixation of the EMA phase. Even so, the value of SF and recovery of EMA/NBR TPVs were still greater than 90% with an increase in strain to 150%, suggesting that the HSMPs still have great application potential under high strain.

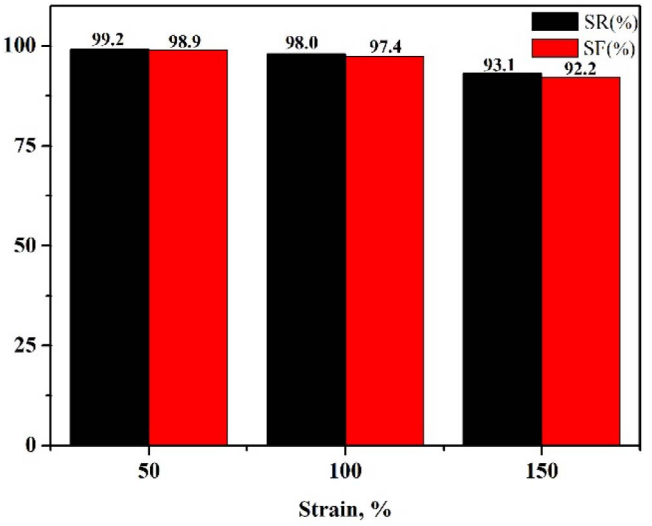

FIG. 11. — SF and SR ratios for the E5N5 specimens obtained at various tensile strain while both T_d and T_r were set at 95 °C.

Downloaded from https://prime-pdf-watermark.prime-prod.pubfactory.com/ at 2025-07-31 via free access

CONCLUSIONS

This work reports the design of HSMPs based on EMA/NBR TPVs. This preparation of HSMPs was easy to carry out using existing apparatuses and has great potential for large-scale fabrication. In addition to the preparation of HSMPs, the HSMP raw materials could be massively supplied at a relatively low cost. The results of shape memory testing showed the appropriate EMA/NBR ratios and high degree of compatibility between the two phases, which would lead to a strong interaction, as shown in the morphology studies. This interaction is an essential factor in obtaining the shape memory performance with high SF and SR. The stress–strain curves at various temperatures showed that with only adequate strain level at the deformation temperature, the shape memory behavior of the EMA/NBR TPVs can be achieved.

ACKNOWLEDGEMENTS

This work was supported by the Shandong Provincial Natural Science Foundation, China (ZR2017MEM021) and an Upgraded Project of Shandong Province for Guidance Ability of Graduate Tutors (SDYY17044).

REFERENCES

[1]W. N. Du, Y. Jin, L. J. Shi, Y. C. Shen, S. Q. Lai, and Y. T. Zhou, *Compos. Part B-Eng*. **195**, 108092 (2020).

[2]S. S. Banerjee and A. K. Bhowmick, RUBBER CHEM. TECHNOL. **88**, 125 (2015).

[3]P. T. Mather, X. Luo, and I. A. Rousseau, *Annu. Rev. Mater. Res*. **39**, 445 (2009).

[4]H. Wang, L. Fang, Z. Zhang, J. Epaarachchi, L. Li, X. Hu, C. Lu, and Z. Xu, *Compos. Part A Appl. S*. **125**, 105525 (2019).

[5]R. A. Bakar, R. Yahya, and S. N. Gan, RUBBER CHEM. TECHNOL. **89**, 465 (2016).

[6]H. Lu, J. Leng, and S. Du, *Smart Mater. Struct*. **18**, 085003 (2009).

[7]Y. J. Liu, H. B. Lv, X. Lan, J. S. Leng, and S. Y. Du, *Compos. Sci. Technol*. **69**, 2064 (2009).

[8]H. Meng and G. Li, *Polymer* **54**, 2199 (2013).

[9]M. Raja, S. H. Ryu, and A. M. Shanmugharaj, *Eur. Polym. J*. **49**, 3492 (2013).

[10]M. Raja, S. H. Ryu, and A. M. Shanmugharaj, *Colloid. Surface A* **450**, 59 (2014).

[11]J. W. Ch, J. W. Kim, Y. C. Jung, and N. S. Goo, *Macromol. Rapid. Comm*. **26**, 412 (2005).

[12]J. S. Leng, X. Lan, Y. J. Liu, S. Y. Du, W. M. Huang, and N. Liu, *Appl. Phys. Lett*. **92**, 014104 (2008).

[13]W. M. Huang, B. Yang, L. An, C. Li, and Y. S. Chan, *Appl. Phys. Lett*. **86**, 114105 (2005).

[14]Y. Kagami, J. P. Gong, and Y. Osada, *Macromol. Rapid. Commun*. **17**, 539 (1996).

[15]X. Xu, P. Fan, J. Ren, Y. Cheng, J. Ren, J. Zhao, and R. Song, *Compos. Sci. Technol*. **168**, 255 (2018).

[16]A. C. de Oliveira Gomes, M. Gomes Oliveira, C. Marcio Paranhos, and B. Guenther Soares, RUBBER CHEM. TECHNOL. **86**, 286 (2013).

[17]S. I. S. M. Reffai and K. Naskar, RUBBER CHEM. TECHNOL. **91**, 357 (2018).

[18]B. G. Soares, J. B. Freitas, A. A. Silva, and A. S. Sirqueira, RUBBER CHEM. TECHNOL. **92**, 546 (2019).

[19]R. Vaia, *Nat. Mater*. **4**, 429 (2005).

[20]S. Samantarai, D. Mahata, A. Nag, G. B. Nando, and N. C. Das, RUBBER CHEM. TECHNOL. **90**, 683 (2017).

[21]Y. Liu, H. Du, L. Liu, and J. Leng, *Smart Mater. Struct*. **23**, 023001 (2014).

[22]N. García-Huete, J. M. Laza, J. M. Cuevas, B. Gonzalo, J. L. Vilas, and L. M. Leon, *J. Polym. Res*. **21**, 481 (2014).

[23]H. Li, X. Gao, and Y. Luo, *Soft Matter* **12**, 3226 (2016).

[24]A. F. Saleeb, S. H. Natsheh, and J. S. Owusu-Danquah, *Polymer* **130**, 230 (2017).

[25]T. Xie, *Nature* **464**, 267 (2010).

[26]J. G. Hardy, M. Palma, S. J. Wind, and M. J. Biggs, *Adv. Mater*. **28**, 5717 (2016).

Downloaded from https://prime-pdf-watermark.prime-prod.pubfactory.com/ at 2025-07-31 via free access

[27]Y. N. Gupta, T. Bhave, M. Chandra, R. B. Sharma, and D. K. Setua, RUBBER CHEM. TECHNOL. **90**, 159 (2017).
[28]P. Yang, G. Zhu, X. Shen, X. Yan, and J. Nie, *RSC Adv*. **6**, 90212 (2016).
[29]S. R. Ryu, J. W. Sung, and D. J. Lee, RUBBER CHEM. TECHNOL. **85**, 207 (2012).
[30]M. D. Hager, S. Bode, C. Weber, and U. S. Schubert, *Prog. Polym. Sci*. **49**, 3 (2015).
[31]Q. Zhao, H. J. Qi, and T. Xie, *Prog. Polym. Sci*. **49**, 79 (2015).
[32]D. G. Yablon, R. Proksch, A. Gannepalli, and A. H. Tsou, RUBBER CHEM. TECHNOL. **85**, 559 (2012).
[33]Y. Meng, X. Huang, C. Fitzgerald, H. Lee, J. C. Yang, and M. Anthamatten, RUBBER CHEM. TECHNOL. **90**, 337 (2017).
[34]Y. Bai, X. Zhang, Q. Wang, and T. Wang, *J. Mater. Chem. A* **2**, 4771 (2014).
[35]L. B. Wang, K. S. Xiong, and Z. B. Wang, *J. Thermoplast. Compos*. **33**, 1217 (2020).
[36]C. Samuel, S. Barrau, J. M. Lefebvre, J. M. Raquez, and P. Dubois, *Macromolecules* **47**, 6791 (2014).
[37]J. A. Gopi and G. B. Nando, RUBBER CHEM. TECHNOL. **88**, 584 (2015).
[38]M. A. Vargas, N. N. Lopez, M. J. Cruz, F. Calderas, and O. Manero, RUBBER CHEM. TECHNOL. **82**, 244 (2009).
[39]J. You, H. Fu, W. Dong, L. Zhao, X. Cao, and Y. Li, *ACS Appl. Mater. Inter*. **4**, 4825 (2012).
[40]A. Mirzadeh, P. G. Lafleur, M. R. Kamal, and C. Dubois, RUBBER CHEM. TECHNOL. **86**, 521 (2013).
[41]D. Yuan, Z. Chen, C. Xu, K. Chen, and Y. Chen, *ACS Sustain. Chem. Eng*. **3**, 2856 (2015).
[42]Y. Chen, K. Chen, Y. Wang, and C. Xu, *Ind. Eng. Chem. Res*. **54**, 8723 (2015).
[43]C. Xu, B. Lin, X. Liang, and Y. Chen, *Ind. Eng. Chem. Res*. **55**, 4539 (2016).
[44]Y. K. Wang, G. M. Zhu, Y. S. Tang, J. Q. Xie, T. T. Liu, and Z. Liu, *J. Polym. Res*. **21**, 405 (2014).
[45]O. Grigoryeva, A. Fainleib, J. Grenet, and J. M. Saiter, RUBBER CHEM. TECHNOL. **81**, 737 (2008).
[46]J. Liang, N. Feng, S. Chang, C. X. Wang, and G. Zhang, RUBBER CHEM. TECHNOL. **86**, 558 (2013).
[47]T. Chung, A. Rorno-Uribe, and P. Mather, *Macromolecules* **41**, 184 (2008).

[*Received July 2020, Revised March 2021*]

Downloaded from https://prime-pdf-watermark.prime-prod.pubfactory.com/ at 2025-07-31 via free access